Induced protein degradation of histone deacetylases 3 (HDAC3) by proteolysis targeting chimera (PROTAC)

Cao, Fangyuan; de Weerd, Sander; Chen, Deng; Zwinderman, Martijn R H; van der Wouden, Petra E; Dekker, Frank J

Published in:
European Journal of Medicinal Chemistry

DOI:
10.1016/j.ejmech.2020.112800

Publication date:
2020

European Journal of Medicinal Chemistry 208 (2020) 112800

Contents lists available at ScienceDirect

European Journal of Medicinal Chemistry

journal homepage: http://www.elsevier.com/locate/ejmech

Research paper

Induced protein degradation of histone deacetylases 3 (HDAC3) by proteolysis targeting chimera (PROTAC)

Fangyuan Cao, Sander de Weerd, Deng Chen, Martijn R.H. Zwinderman, Petra E. van der Wouden, Frank J. Dekker*

Chemical and Pharmaceutical Biology, Groningen Research Institute of Pharmacy, University of Groningen, the Netherlands

ARTICLE INFO

Article history:
Received 5 May 2020
Received in revised form
4 August 2020
Accepted 27 August 2020
Available online 6 September 2020

Keywords:
Proteolysis targeting chimera (PROTAC)
Class I histone Deacetylases (HDACs)
Cereblon (CRBN) ligand
NF-κB subunit p65
Pomalidomide

ABSTRACT

Histone deacetylases (HDACs) play important roles in inflammatory diseases like asthma and chronic obstructive pulmonary disease (COPD). Unravelling of and interfering with the functions of specific isoenzymes contributing to inflammation provides opportunities for drug development. Here we synthesize proteolysis targeting chimeras (PROTACs) for degradation of class I HDACs in which *o*-aminoanilide-based class I HDAC inhibitors are tethered to the cereblon ligand pomalidomide. One of these PROTACs, denoted HD-TAC7, showed promising degradation effects for HDAC3 with a DC_{50} value of 0.32 μM. In contrast to biochemical evidence using siRNA, HD-TAC7 showed a minimal effect on gene expression in LPS/IFNγ-stimulated RAW 264.7 macrophages. The lack of effect can be attributed to downregulation of the NF-κB subunit p65, which is a known side effect of pomalidomide treatment. Altogether, we describe a novel PROTAC that enables selective downregulation of HDAC3 levels, however we note that concomitant downregulation of the NF-κB subunit p65 can confound the biological outcome.

1. Introduction

Acetylation of lysine residues of cellular proteins plays a key role in the regulation of cellular signal transduction pathways. The turnover of lysine acetylation of histone proteins as well as non-histone proteins is regulated by lysine deacetylases such as the histone deacetylases (HDACs) and lysine acetyl transferases such as histone acetyl transferases (HATs). Currently, eighteen HDAC isoenzymes, which can be divided into four classes, have been discovered. The classes I, II, and IV contain the zinc-dependent HDACs 1–11, while class III consists of the NAD + -dependent sirtuins (SIRT1-7) [1,2]. Among them, class I HDACs, containing HDAC1, 2, 3 and 8, are well-known for their importance in cell motility, immunoregulation, and proliferation [3]. In order to exploit these enzymes in drug discovery it is important to identify the roles of these enzymes in pathology.

Several reports have shown that the class I HDACs 1, 2 and 3 are involved in immune responses [4–6]. HDACs can affect the acetylation status of transcription factors involved in inflammation, such as NF-κB. Stability and DNA binding capability of NF-κB are influenced by its acetylation status (as reviewed [7–9]). Consequently, HDAC inhibition could affect NF-κB acetylation, which in turn influences expression of inflammatory genes. Previously, we reported anti-inflammatory activity for the HDAC1,2, and 3 selective inhibitor Entinostat both *in vitro* and *in vivo*, which is connected to upregulation of the anti-inflammatory cytokine Interleukin-10 (IL-10) [10]. Mechanistically this could be linked to increased acetylation, nuclear localization and IL-10 promotor binding by the p65 subunit of the NF-κB transcription factor. Interestingly, siRNA mediated knockdown of HDAC3 upregulated expression of IL-10 in lipopolysaccharides (LPS)/interferonγ (IFNγ) treated RAW 264.7 macrophages [11]. In contrast, the HDAC3 selective inhibitor, RGFP966, did not show significant effects on gene expression in RAW 264.7 macrophages [12]. This discrepancy between siRNA mediated knockdown and HDAC3 selective inhibition of deacetylase activity suggests that this proteins functions as a scaffold rather than as a catalyst in inflammatory signaling.

These results indicate that HDAC isoenzymes have potential in drug discovery but that inhibition of the HDAC3 isoenzyme using an HDAC3 selective inhibitor is not sufficient to induce an anti-inflammatory effect. This problem might be resolved by a novel strategy that utilizes “Proteolysis targeting chimera (PROTAC)” to

* Corresponding author.
E-mail address: f.j.dekker@rug.nl (F.J. Dekker).

https://doi.org/10.1016/j.ejmech.2020.112800
0223-5234/

"hijack" the natural ubiquitin proteasome system (UPS) for degradation of HDAC3 [13,14]. Towards this aim, PROTACs were designed by covalent linkage of a selective HDAC inhibitor to a ligand for E3 ubiquitin ligase that are connected via a linker of variable length. Binding of the PROTACs to both the HDAC and the E3 ligase induces the formation of a ternary complex. Formation of this complex triggers subsequent ubiquitination of the target protein and degradation through the UPS [13,15,16]. To date, the reported PROTACs mainly contain ligands for E3 ligases such as Cereblon (CRBN) and Von Hippel-Lindau (VHL) that enable recruitment of E3 ligase activity to the target protein [16,17]. Considering this, PROTACs can provide interesting novel tools to study the functional behavior of HDACs [18], which could ultimately provide conceptual novel opportunities for drug discovery [13,19].

Prior studies report that PROTAC mediated degradation of HDACs is feasible for class II HDAC6 [20–22] and class III HDAC sirtuin 2 [23]. All the reported HDAC targeting PROTACs contain pomalidomide derivatives as E3 ligase to recruit Cereblon for targeted protein degradation. This indicates that Cereblon can be used as E3 ligase to design PROTACs for HDAC family enzymes.

Substituted *o*-aminoanilide derivatives bind specifically to the active site of class I HDACs 1, 2 and 3 [24,25]. Two of these inhibitors, Entinostat and CI994, are currently in clinical trials. Entinostat is in phase II clinical trials, while CI994 is in phase III clinical trials [26] (Fig. 1A). In addition, the *o*-aminoanilide core provides slow-tight binding [27,28], which might be beneficial for the development of PROTACs. Therefore, we applied *o*-aminoanilide as a class I HDAC binding motif to obtain ligands targeting the active site of HDAC1, 2 and 3. By including pomalidomide as Cereblon E3 ligase ligand, a series of HDAC-PROTACs (HD-TACs) were synthesized in which the length of the linker between the HDAC inhibitor and the Cereblon ligand were varied (Fig. 1B). Here, we report a novel class of class I HDAC directed PROTACs that include *o*-aminoanilide-based class I HDAC ligands and pomalidomide as ligand for CRBN E3 ligase.

2. Results and discussion

2.1. Chemistry

The synthetic routes towards the HD-TACs are outlined in Scheme 1. The ligands for HDAC **2a** and **2b** were synthesized starting from Boc-protected *ortho*-amino aniline or Boc-protected *para*-fluoro *ortho*-amino aniline. These building blocks were linked to 4-nitrobenzoyl chloride following reported procedures [29,30]. Subsequently, the nitro-group was reduced to an amine using palladium on carbon (Pd/C) under hydrogen atmosphere to afford **3a** and **3b** with yields of 42% and 53%, respectively. A condensation reaction was applied to couple intermediate **3a** with benzyloxycarbonyl (Cbz) protected amino acid linkers using EDCI and HOBt as reagents to obtain intermediates **4a-4c** in yields between 40 and 60%, while intermediate **3b** was used to obtain intermediate **4d** using the same method with a yield of 56%. The Cbz protective group was removed by hydrogenolysis using Pd/C as a catalyst to afford compounds **5a-5d** with yield between 95 and 99%. Subsequently, **5a-5d** were linked to the CRBN E3 ligase ligands using either 2-(2,6-dioxopiperidin-3-yl)-4-fluoroisoindoline-1,3-dione or (2-(2,6-dioxopiperidin-3-yl)-1,3-dioxoisoindolin-4-yl) glycine using previously described procedures [31,32]. The compounds **6a-6d** were achieved by coupling compounds **5a-5d** with (2-(2,6-Dioxopiperidin-3-yl)-1,3-dioxoisoindolin-4-yl)glycine employing an amidation reaction. The following Boc-deprotection of compounds **6a-6d** provided compounds **7a-7d** (code with HD-TAC6, HD-TAC1, HD-TAC5 and HD-TAC7, Scheme 1). Compounds **8a-8c** were formed by substitution reaction of 2-(2,6-dioxopiperidin-3-yl)-4-fluoroisoindoline-1,3-dione with compounds **5a-5c**. The subsequent Boc-deprotection of compounds **8a-8c** afforded the compounds **9a**–**9c** (code with HD-TAC4, HD-TAC2 and HD-TAC3).

2.2. Biological evaluation

The compounds synthesized above were subjected to HDAC inhibition studies using HDAC1, 2 and 3, which provided IC_{50} values that are similar to the IC_{50} values of CI994 (Table 1). These result indicate that class I HDAC binding is retained for these HD-TACs. The effects on cell viability were investigated and showed that more than 80% of RAW264.7 macrophages survived treatment with HD-TAC1-6 at concentrations up to 10 μM for 24h. Furthermore, HD-TAC1-6 proved to be less toxic than CI994, which inhibited cell proliferation by 30% upon treatment with 3 μM for 24h (Figure S2).

PROTACs can have highly specific effects on degradation of their targets, because they need to form stable protein ternary complexes to provide the proper protein-protein interactions between the E3 ubiquitin ligase and the target protein for ubiquitination and subsequent degradation [12,26–28]. Therefore, the linker length between the E3 ligase ligand and the target protein ligands needs to be optimized to improve the potency and selectivity of HDAC degradation [32,33,34]. Towards this aim, a series of HD-TACs with a variable linker length was synthesized and their potency to degrade HDACs in macrophages was investigated. We performed a screening of HD-TACs with different linker lengths at 10 μM for 24h in RAW264.7 macrophages. Using western blot the protein levels were analyzed (Fig. 2), which demonstrated an interesting pattern of selectivity and potency with respect to HDAC degradation. Although all the HD-TACs bind to HDAC1, none of these HD-TACs obviously triggered HDAC1 degradation. HD-TAC3 and HD-TAC5 triggered the most obvious degradation of HDAC2, whereas HD-TAC1 and 4 only triggered degradation of HDAC3. Among the amide-containing HD-TACs, HD-TAC1 and 5 provided HDAC3 degradation, while HD-TAC6 did not. This difference can be attributed to the shorter linker in HD-TAC6 compared to HD-TAC1 and 5. Although HD-TAC3, 4 and 5 triggered degradation of HDAC3, both the potency and selectivity of HD-TAC1 appeared to be the best. Therefore, HD-TAC1 was chosen as a starting point to develop a selective HDAC3 degrading PROTAC. Subsequently, we tested the degradation potency and selectivity of HD-TAC1 among HDACs 1, 2 and 3 using concentrations ranging from 1 μM to 100 μM (data on cell viability are shown in the supporting information). The concentration dependence shows HDAC3 degradation by HD-TAC1 at concentrations of 10 μM and higher. This might be due to differences in sub-cellular localization among HDAC1, 2 and 3. HDAC1 and 2 are mainly located in the nucleus, while HDAC3 is located both in the nucleus and cytoplasm [35]. However, at concentrations of 30 μM and higher degradation of HDAC1 was observed, whereas HDAC2 degradation was only observed at 100 μM. We also tested the HDAC3 degradation effect with HD-TAC1 in A549 cells, however, in these cells HDAC3 degradation was not observed in concentrations up to 50 μM (Figure S5). This indicates that PROTAC mediated degradation also depends on the cell type under investigation [20,31]. Taken together, we demonstrated that the linker length drives the selectivity among these HD-TACs, and HD-TAC1 showed selective HDAC3 degradation at a lower concentration, whereas this selectivity was not observed at higher concentrations.

HD-TAC1 was used as a starting point to gain selectivity among HDAC1, 2 and 3. Towards this aim, we modified the *o*-aminoanilide with a fluorine atom (HD-TAC7), which is known to increase HDAC3 inhibitory selectivity [24]. The inhibitory potency among HDACs 1, 2 and 3 was investigated and showed that HD-TAC7 gained

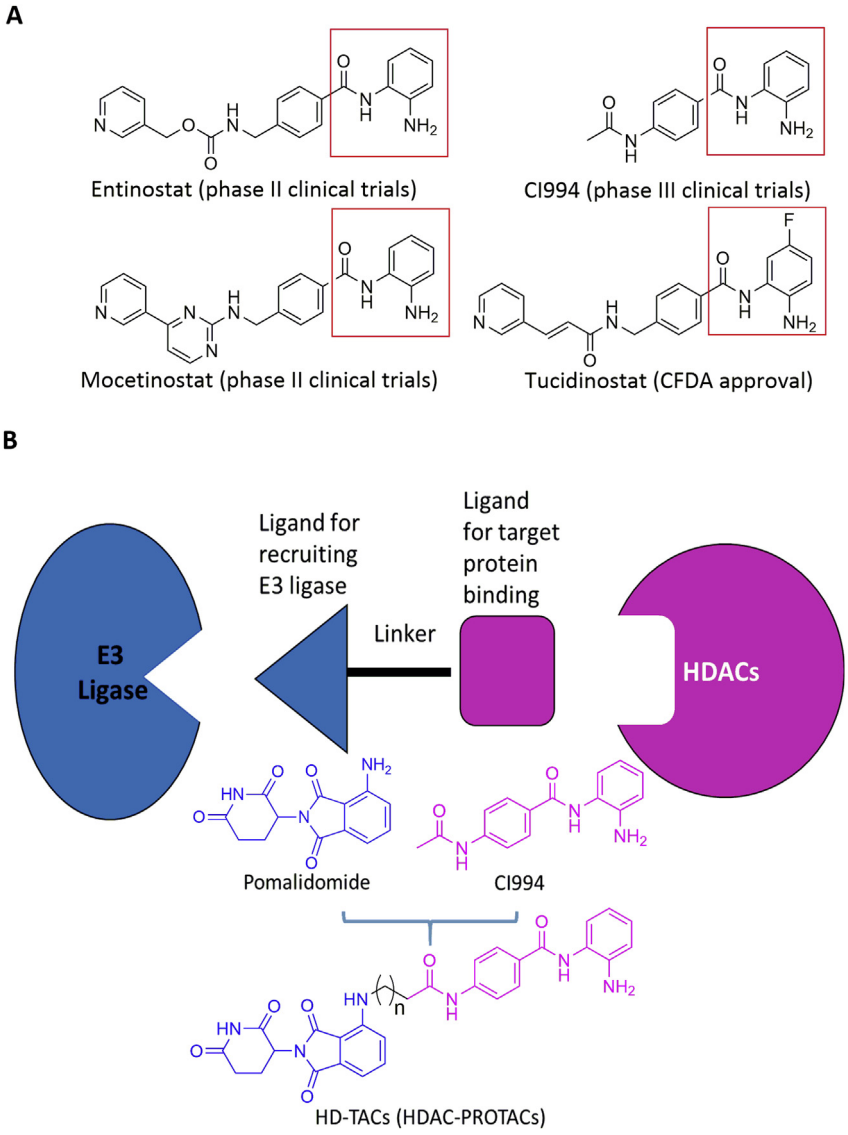

Fig. 1. (A) Chemical structures of representative *o*-aminoanilide derivatives as class I HDAC inhibitors (*o*-aminoanilide scaffold is marked in orange). (B) Conceptual PROTAC design for targeting HDACs and design of the class I HDAC PROTACs. (For interpretation of the references to colour in this figure legend, the reader is referred to the Web version of this article.)

selectivity for HDAC3 (Table 2).

The concentration dependence of HD-TAC7 towards HDAC1, 2 and 3 degradation in RAW 264.7 cells was investigated (Fig. 3A). HD-TAC7 mediated degradation of HDAC3 with a DC_{50} (50% degradation concentration) value of 0.32 μM as identified by protein quantification upon western blot analysis (Fig. 3B). For HDAC1 and 2 no significant degradation was observed. A time-dependent analysis of HD-TAC7 treatment of RAW 264.7 cells displayed fast response in cells, and HD-TAC7-induced HDAC3 degradation reached the maximal effect at 6h and lasted at least 48h (Fig. 3C and D). To explore whether HD-TAC7 affected histone acetylation level in macrophages, we tested HDAC3-mediated histone3 lysine27(H3K27) acetylation level using western blot [36]. As shown in Fig. 3E and F, HD-TAC7 induced an increase of H3K27 acetylation in RAW 264.7 macrophages.

Further experiments were done to confirm the importance of both the HDAC ligand as well as the Cereblon ligand for the observed HDAC3 degradation. Cells were treated with free pomalidomide or CI994 to compete with the HD-TAC for binding to CRBN or HDAC respectively. Cells were pre-treated with pomalidomide or CI994 for 1h, followed by addition of HD-TAC7 for combination treatment during 24h (Fig. 4A and B). Both combined treatment of HD-TAC7 with pomalidomide or CI994 rescued HDAC3 degradation, indicating that degradation of HDAC3 by HD-TAC7 is Cereblon-dependent. The proteasome inhibitor Bortezomib also completely blocked the degradation of HDAC3 by HD-TAC7 (Fig. 4C), indicating that HDAC3 degradation by HD-TAC7 depends on proteasome activity. These data provide evidence that HD-TAC7 induces E3 ligase dependent ubiquitination and subsequent proteasome mediated HDAC3 degradation.

Subsequently, we investigated the effect of HD-TAC7 treatment on pro- and anti-inflammatory gene transcription in RAW 264.7 cells. We employed LPS/IFNγ-stimulated RAW 264.7 cells to monitor the transcription of tumor necrosis factor α (TNFα), interleukin-6 (IL-6) and inducible nitric oxide synthase (iNOS) as pro-inflammatory genes and the transcription of IL-10 as anti-inflammatory gene [10,12]. As observed previously, Entinostat increased the expression of both pro- and anti-inflammatory genes,

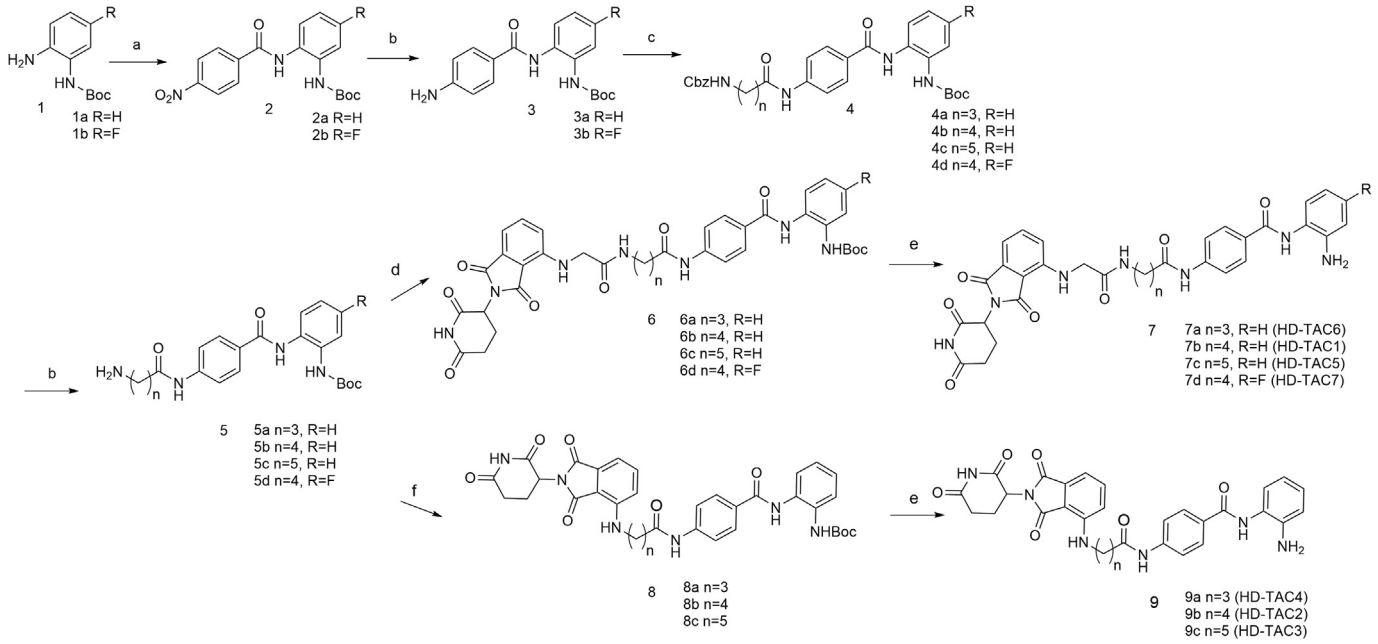

Scheme 1. Reaction conditions: (a) 4-nitrobenzoyl chloride, Et_3N, DCM, r.t.; (b) H_2, Pd/C, methanol, r.t.; (c) Cbz-protected aliphatic carboxylic acids, EDCI, HOBt, DCM, Et_3N, r.t.; (d) (2-(2,6-Dioxopiperidin-3-yl)-1,3-dioxoisoindolin-4-yl)glycine, EDCI, HOBt, DCM, Et_3N, r.t.; (e) TFA, DCM, r.t.; (f) 2-(2,6-dioxopiperidin-3-yl)-4-fluoroisoindoline-1,3-dione, DIPEA, DMF, 80 °C.

Table 1
Binding affinities of HD-TACs.

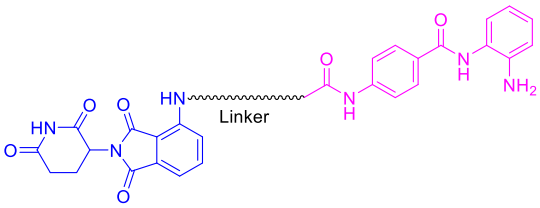

Name	Linker	HDAC IC_{50} (μM±SD)		
		HDAC1	HDAC2	HDAC3
CI994	–	0.13 ± 0.01	0.83 ± 0.14	0.19 ± 0.02
HD-TAC1(**7b**)	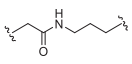	0.29 ± 0.01	0.62 ± 0.04	0.52 ± 0.06
HD-TAC2(**9b**)		0.42 ± 0.03	1.0 ± 0.07	1.0 ± 0.09
HD-TAC3(**9c**)	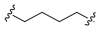	0.22 ± 0.02	0.97 ± 0.12	0.54 ± 0.08
HD-TAC4(**9a**)		0.36 ± 0.03	1.2 ± 0.08	0.87 ± 0.1
HD-TAC5(**7c**)	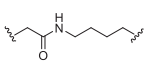	0.24 ± 0.03	0.75 ± 0.05	0.33 ± 0.03
HD-TAC6(**7a**)	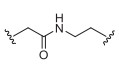	0.32 ± 0.02	1.5 ± 0.1	0.56 ± 0.07

and CI994 showed a similar profile (Fig. 5). However, HD-TAC7 did not show significant effects on IL-10 gene expression, which is not in line with the biochemical evidence from previous work. In our previous work, we found that siRNA knockdown of HDAC3 increased IL-10 gene expression [11]. In addition, treatment with the class I selective HDAC inhibitor Entinostat upregulated IL-10 gene expression, which could be connected to increased NF-κB p65 acetylation, increased p65 nuclear localization and increased binding to the IL-10 promoter [10]. HD-TAC7 showed a similar influence on all the pro- and anti-inflammatory gene transcription levels as pomalidomide. It was reported that pomalidomide decreased the NF-κB p65 concentration and promoted the chemosensitization of pancreatic cancer in human pancreatic cancer cells [37]. We suspected that the failure to reproduce the results from siRNA mediated knockdown of HDAC3 using a PROTAC might be attributed to the effect of the CRBN ligand pomalidomide on the expression levels of the NF-κB transcription factor. Therefore, we analyzed the NF-κB p65 protein level in HD-TAC7 treated RAW 264.7 cells, together with pomalidomide and CI994 as control (Fig. 6A). Interestingly, both treatments with HD-TAC7 and pomalidomide provide downregulation of NF-κB p65 in RAW 264.7 macrophages. Considering that NF-κB p65 is an active transcription factor of IL-10 [10] the downregulation of NF-κB p65 could be the reason that HD-TAC7 failed to increase IL-10 gene transcription. Apparently, the use of pomalidomide as cereblon E3 ligase ligand in PROTACs can downregulate NF-κB p65, thus interfering with NF-κB signaling. We also tested the potency of pomalidomide analogs, such as thalidomide and lenalidomide, in the regulation of NF-κB p65 protein expression level. As shown in Fig. 6B, pomalidomide analogs also downregulate the NF-κB p65 levels, which indicates that pomalidomide analogs can not be used to alleviate the problem of NF-κB p65 downregulation. Taken together, it is important to note that the effects of pomalidomide and its analogs on the NF-κB p65 subunit should be taken into consideration when designing PROTACs directed at HDAC family enzymes or other proteins.

3. Conclusion

In this study, we reported the development of a novel PROTAC for HDAC3 degradation by tethering the CRBN ligand pomalidomide and *o*-aminoanilide-based class I HDAC inhibitors. By varying the length of the linker between both ligands, we were able to identify HD-TAC1, which degraded HDAC3 at 10 μM concentration in RAW 264.7 macrophages, whereas HDAC1 and 2 were also degraded at higher concentrations. Apparently, even nuclear

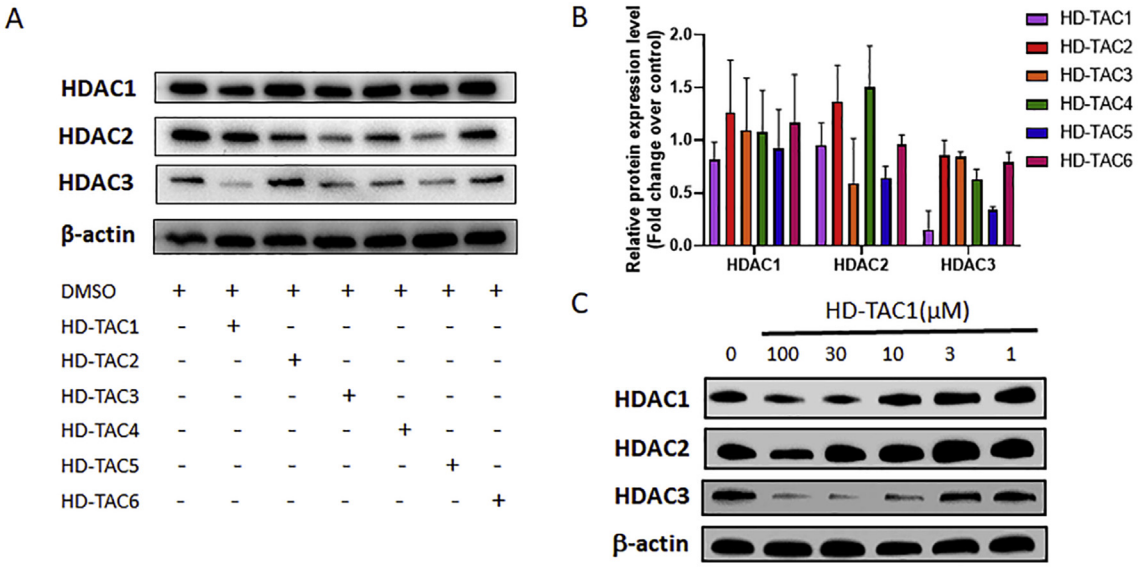

Fig. 2. (A) Analysis of the HDAC1, HDAC2 and HDAC3 protein levels upon treatment with HD-TAC1-6 at 10 μM in RAW 264.7 macrophages. (B) The bands of Fig. 2A were quantified using Image J and plotted. Average and standard deviations of 2 independent experiments are plotted as fold of the untreated control. (C) Western blot analysis of the HDAC1, HDAC2 and HDAC3 protein levels upon treatment of RAW 264.7 macrophages with HD-TAC1 using a range of HD-TAC1 concentrations for 24h.

Table 2
Binding affinities of HD-TAC1 and HD-TAC7.

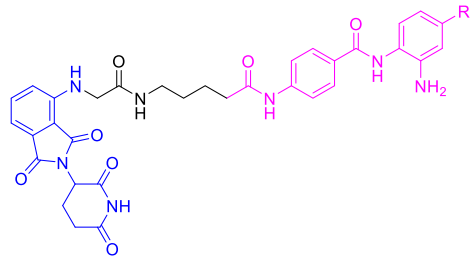

Name	R	HDAC IC_{50} (μM±SD)		
		HDAC1	HDAC2	HDAC3
HD-TAC1(**7b**)	H	0.29 ± 0.01	0.62 ± 0.04	0.52 ± 0.06
HD-TAC7(**7d**)	F	3.6 ± 0.5	4.2 ± 0.9	1.1 ± 0.1

enzymes such as HDAC1 and 2 can be degraded by PROTAC treatment. We note that the effectiveness of the PROTAC mediated degradation depends on the type of cell line used, since we did not observe HDAC3 degradation in A549 cells. HDAC3 selectivity was improved by using a *para*-fluoro *ortho*-amino anilide core to provide HD-TAC7. HD-TAC7 showed improved potency and selectivity for HDAC3 degradation compared to HD-TAC1 and reached a DC_{50} value of 0.32 μM in RAW 264.7 macrophages. Controls confirmed that degradation disappears upon competition with the HDAC ligand as well as the CRBN E3 ligase ligand. Application of HD-TAC7 in LPS/IFNγ stimulated RAW 264.7 macrophages showed that HD-TAC7 did not significantly affect gene transcription of IL-10, iNOS, IL-6 and TNFα in contrast to the HDAC inhibitors Entinostat and CI994. The lack of effect might be caused by a side effect of treatment with the pomalidomide CRBN E3 ligase ligand since it downregulates the levels of the NF-κB p65 subunit. Thus, PROTACs using this ligand will unintendedly interfere with signaling via this pathway, which plays crucial roles in many processes. Taken together, our results contribute to understanding the parameters important for PROTAC design, which provides a basis for further development this novel type of molecular tools for applications in cell-based studies and ultimately drug discovery.

4. Experimental section

4.1. Chemistry

General. The solvents and reagents were purchased from Sigma-Aldrich, Acros chemicals or abcr GmbH without further purification. Reactions were monitored by thin layer chromatography (TLC). Merck silica gel 60 F254 plates were used and spots were detected under UV light or after staining with potassium permanganate for the non UV-active compounds. MP Ecochrom silica 32–63, 60 Å was used for flash column chromatography. ^{1}H NMR (500 MHz) and ^{13}C NMR (126 MHz) spectra were recorded with a Bruker Avance 4-channel NMR Spectrometer with TXI probe. Chemical shifts were referenced to the residual proton and carbon signal of the deuterated solvent $CDCl_3$: δ = 7.26 ppm (^{1}H) and 77.05 ppm (^{13}C), $(CD_3)_2SO$: δ = 2.50 ppm (^{1}H) and 39.52 ppm (^{13}C) CD_3OD: δ = 3.31 ppm (^{1}H) and 49.00 ppm (^{13}C). The following abbreviations were used for spin multiplicity: s = singlet, br. s = broad singlet, d = doublet, t = triplet, q = quartet, p = quintet, dd = double of doublets, ddd = double of doublet of doublets, m = multiplet. Fourier Transform Mass Spectrometry (FTMS) was recorded on an Orbitrap XL Hybrid Ion Trap-Orbitrap Mass Spectrometer to give high-resolution mass spectra (HRMS). High-performance liquid chromatography (HPLC) analysis was performed for confirming purity with a Shimadzu LC-20AD HPLC, with a Shimadzu SP-M20A ELSD detector, and with a Shimadzu SPD-M20A photodiode array detector. Analytical HPLC was performed using a Kinetex C18 column (150 mm × 4.6 mm, 5 μm) with 15–100% MeCN gradient in H_2O as a mobile phase. Retention time (RT) of HPLC was also reported.

4.1.1. Synthetic procedure 1: amide bond formation

A carboxylic acid derivative (1.0 equiv) was dissolved in dry CH_2Cl_2 (5.0 mL) and cooled on an ice bath. The coupling reagents EDCI (1.2 equiv) and HOBt (0.4 equiv) were added to the solution and the reaction was stirred on ice for 15 min. Then Et_3N (2.0 equiv)

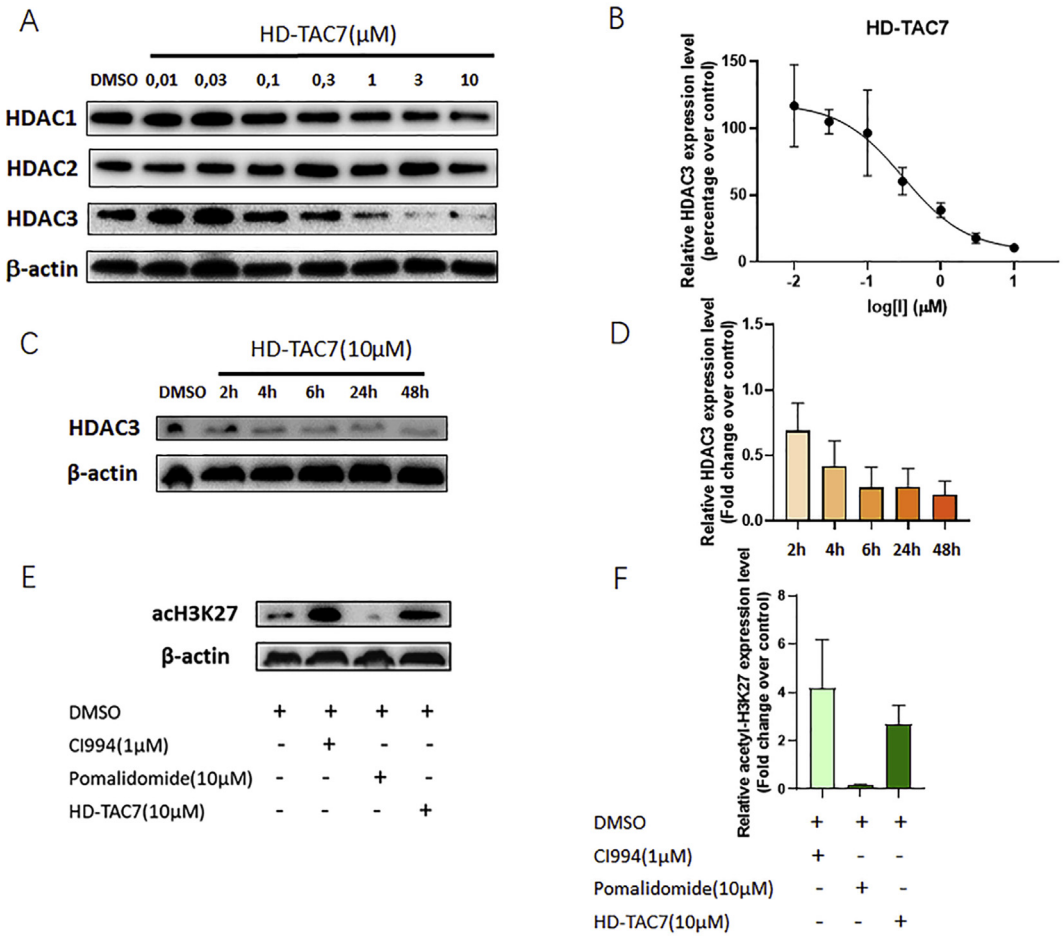

Fig. 3. (A) Analysis of HDAC1, HDAC2 and HDAC3 degradation upon HD-TAC7 treatment of RAW 264.7 macrophages for 24 h using Western blot. (B) The bands of Fig. 3A were quantified using Image J and plotted in a graph, which was used for determination of the 50% degradation concentration by non-linear curve fitting with GraphPad Prism. Average and standard deviations of 2–3 independent experiments are plotted as percentage of the untreated control. (C) Analysis of HDAC3 degradation upon HD-TAC7 treatment of RAW 264.7 macrophages for indicated time point using Western blot. (D) The bands of Fig. 3C were quantified using Image J and plotted. Average and standard deviations of 2 independent experiments are plotted as fold of the untreated control. (E) Analysis of acetylation level of lysine 27 on histone 3 upon CI994, Pomalidomide and HD-TAC7 treatment of RAW 264.7 macrophages for 24h using Western blot. (F) The bands of Fig. 3E were quantified using Image J and plotted. Average and standard deviations of 2 independent experiments are plotted as fold of the untreated control.

and the amine (1.0 equiv) were added subsequently to the mixture, and it was stirred at room temperature overnight. The reaction mixture was washed with 1.0 M aqueous HCl (10 mL), saturated aqueous $NaHCO_3$ (10 mL), and brine (10 mL); dried over $MgSO_4$; filtered; and concentrated under reduced pressure. The crude product was purified by flash column chromatography and eluted with 20% ethyl acetate in petroleum ether as a solvent to obtain a white solid product in yields between 40 and 65%.

4.1.2. Synthetic procedure 2: reduction reaction

Compounds containing a nitro or Cbz-protective group (1.0 equiv) were dissolved in methanol (3 mL). The solution was added to Pd/C (0.1 equiv) and the flask was charged with hydrogen (H_2) gas. The reaction mixture was stirred at r.t. and detected with TLC for a period from 2 h to 18 h until the solution became homogeneous. Finally, the reaction mixture was filtered through Celite and evaporated under reduced pressure to obtain the final product without further purification.

4.1.3. Synthetic procedure 3: nucleophilic substitution reaction

Boc protected alkyl amines (**5a-5c**) (1.1 equiv) were added to a stirred solution of 2-(2,6-dioxopiperidin-3-yl)-4-fluoroisoindoline-1,3-dione (1.0 equiv) in DMF (3.0 mL) and DIPEA (2.0 equiv). The reaction mixture was stirred at 80 °C for 12h. Then the mixture was cooled to room temperature, poured into cold brine and extracted with EtOAc (3 times, 10 mL). The organic layers were combined, washed with cold brine and dried over $MgSO_4$. After filtration and evaporation, the crude residue was purified by flash column chromatography and eluted with 5% methanol in CH_2Cl_2 to obtain the product with yields ranging from 30 to 60%.

4.1.4. Synthetic procedure 4: boc deprotection

A Boc-protected compound (1.0 equiv.) was dissolved in CH_2Cl_2 (chemical pure, 1.5 mL). Subsequently, Trifluoroacetic acid (TFA, 1.5 mL) was added. The mixture was stirred at r.t. until the solution became homogeneous. The mixture was extracted with 1.0 M NaOH (20 mL). The organic layer was collected and dried over $MgSO_4$, removal of the solvent under reduced pressure afforded the final product.

4.1.5. tert-Butyl (2-(4-nitrobenzamido)phenyl)carbamate (2a)

tert-Butyl(2-aminophenyl)carbamate (2.08 g, 10 mmol) and Et_3N (2.8 mL, 20 mmol) were added in CH_2Cl_2 (10 mL), which was cooled to 0 °C. Then, 4-nitrobenzoyl chloride (1.9 g, 10 mmol) was dissolved in CH_2Cl_2 (3 mL) and added dropwise to the mixture. Subsequently, the reaction was stirred at room temperature

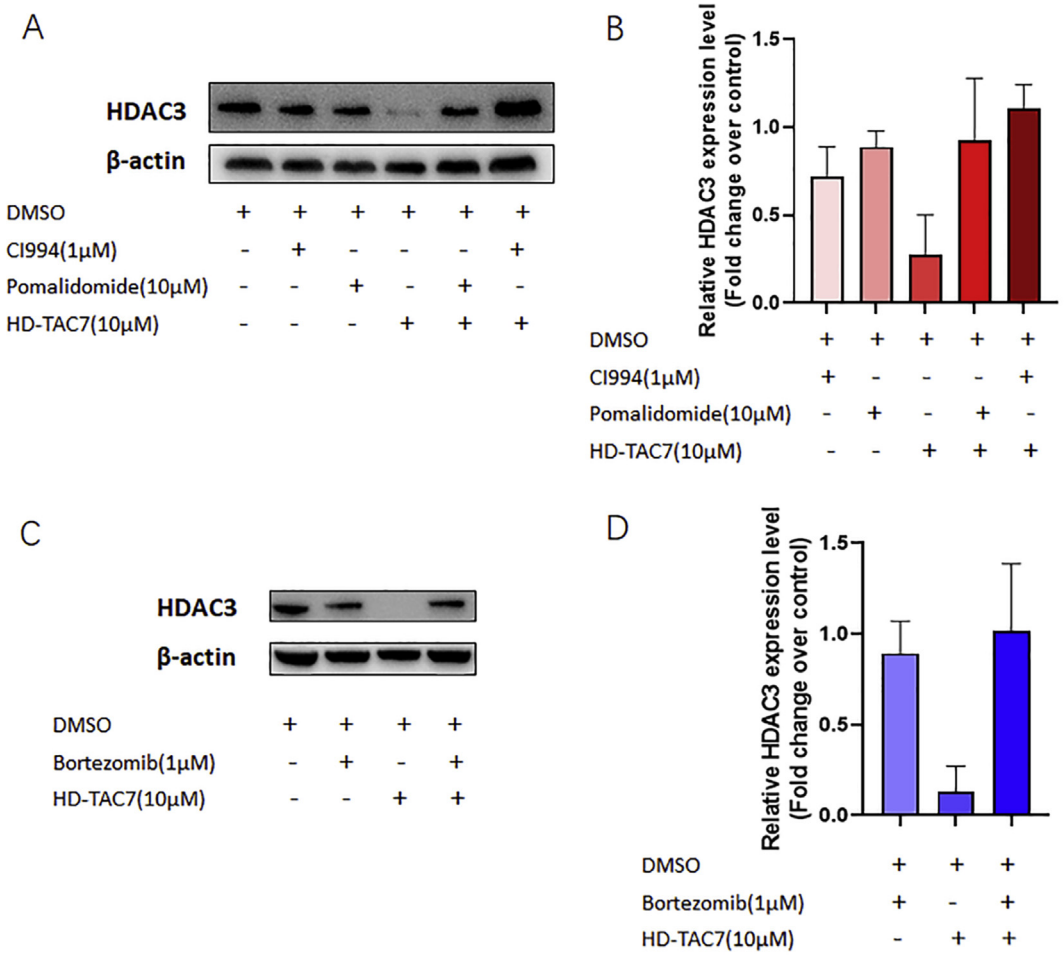

Fig. 4. (A) Analysis of the HDAC3 protein levels in RAW 264.7 macrophages. The cells were pre-treated with pomalidomide or CI994 for 1h followed by addition of HD-TAC7 for combination treatment during 24h, while the control cells were treated with CI994 or pomalidomide for 25h. (B) The bands of Fig. 4A were quantified using Image J and plotted. Average and standard deviations of 2 independent experiments are plotted as fold of the untreated control. (C) Analysis of the HDAC3 protein levels in RAW 264.7 macrophages. The cells were treated with Bortezomib, HD-TAC7 or the combination of Bortezomib and HD-TAC7 for 24h. (D) The bands of Fig. 4C were quantified using Image J and plotted. Average and standard deviations of 2 independent experiments are plotted as fold of the untreated control.

overnight. Then, the reaction mixture was washed with a saturated aqueous $NaHCO_3$ solution (10 mL), a 1.0 M aqueous HCl solution (10 mL), and brine (10 mL). The organic layer was dried over $MgSO_4$, filtered and concentrated under reduced pressure. The crude product was obtained as yellow solid in an estimated yield of 91% and used for the next step without further purification. ^{1}H NMR (500 MHz, Chloroform-*d*) δ 9.78 (s, 1H), 8.32 (d, J = 8.8 Hz, 2H), 8.15 (d, J = 8.7 Hz, 2H), 7.91 (d, J = 8.0 Hz, 1H), 7.29 (t, J = 7.7 Hz, 1H), 7.20 (d, J = 7.8 Hz, 1H), 7.13 (d, J = 7.3 Hz, 1H), 6.70 (s, 1H), 1.53 (s, 9H).

4.1.6. tert-Butyl (2-(4-aminobenzamido)phenyl)carbamate(3a)

The product was obtained using synthetic procedure 2, starting from compound **2a**. Yellow oil, yield 99%.^{1}H NMR (500 MHz, Chloroform-*d*) δ 8.76 (s, 1H), 7.79 (d, J = 8.6 Hz, 2H), 7.71 (d, J = 7.8 Hz, 1H), 7.31 (d, J = 7.9 Hz, 1H), 7.23–7.13 (m, 2H), 6.82 (s, 1H), 6.70 (d, J = 8.6 Hz, 2H), 4.02 (s, 2H), 1.51 (s, 9H).

4.1.7. Benzyl (4-((4-((2-((tert-butoxycarbonyl)amino)phenyl) carbamoyl)phenyl)amino)-4-oxobutyl)carbamate(4a)

The product was obtained using synthetic procedure 1, starting from compound **3a**. White solid, yield 42%. ^{1}H NMR (500 MHz, Chloroform-*d*) δ 9.03 (s, 1H), 8.76 (s, 1H), 7.94 (d, J = 8.6 Hz, 2H), 7.81 (d, J = 7.9 Hz, 1H), 7.73 (d, J = 8.4 Hz, 2H), 7.37 (d, J = 2.6 Hz, 4H), 7.30–7.27 (m, 1H), 7.26–7.21 (m, 2H), 7.18 (td, J = 7.6, 1.5 Hz, 1H), 6.72 (s, 1H), 5.14 (s, 2H), 4.99 (d, J = 13.1 Hz, 1H), 3.40–3.31 (m, 2H), 2.47–2.38 (m, 2H), 1.93 (p, J = 6.3 Hz, 2H), 1.52 (s, 9H).

4.1.8. tert-Butyl (2-(4-(5-(((benzyloxy)carbonyl)amino) pentanamido)benzamido)phenyl)carbamate(4b)

The product was obtained using synthetic procedure 1, starting from compound **3a**. White solid, yield 53%.^{1}H NMR (500 MHz, Methanol-d_4) δ 7.94 (d, J = 8.7 Hz, 2H), 7.74 (d, J = 8.7 Hz, 2H), 7.61–7.57 (m, 1H), 7.45–7.41 (m, 1H), 7.33 (q, J = 7.9, 7.3 Hz, 4H), 7.29–7.25 (m, 1H), 7.23 (ddd, J = 6.9, 4.2, 2.0 Hz, 2H), 5.07 (s, 2H), 3.17 (t, J = 6.9 Hz, 2H), 2.43 (t, J = 7.4 Hz, 2H), 1.73 (p, J = 7.4 Hz, 2H), 1.58 (dt, J = 14.0, 7.0 Hz, 2H), 1.50 (s, 9H).

4.1.9. Benzyl (6-((4-((2-((tert-butoxycarbonyl)amino)phenyl) carbamoyl)phenyl)amino)-6-oxohexyl)carbamate(4c)

The product was obtained using synthetic procedure 1, starting from compound **3a**. White solid, yield 40%.^{1}H NMR (500 MHz, Chloroform-*d*) δ 9.10 (s, 1H), 7.93 (d, J = 8.5 Hz, 2H), 7.80 (d, J = 7.8 Hz, 1H), 7.64 (d, J = 8.2 Hz, 2H), 7.50 (s, 1H), 7.38–7.27 (m, 5H), 7.24 (d, J = 7.7 Hz, 2H), 7.17 (td, J = 7.6, 1.5 Hz, 1H), 6.74 (s, 1H), 5.09 (s, 2H), 4.81 (s, 1H), 3.22 (q, J = 6.8 Hz, 2H), 2.37 (t, J = 7.4 Hz, 2H), 1.77 (q, J = 7.6 Hz, 2H), 1.57 (d, J = 7.1 Hz, 2H), 1.52 (s, 9H), 1.41

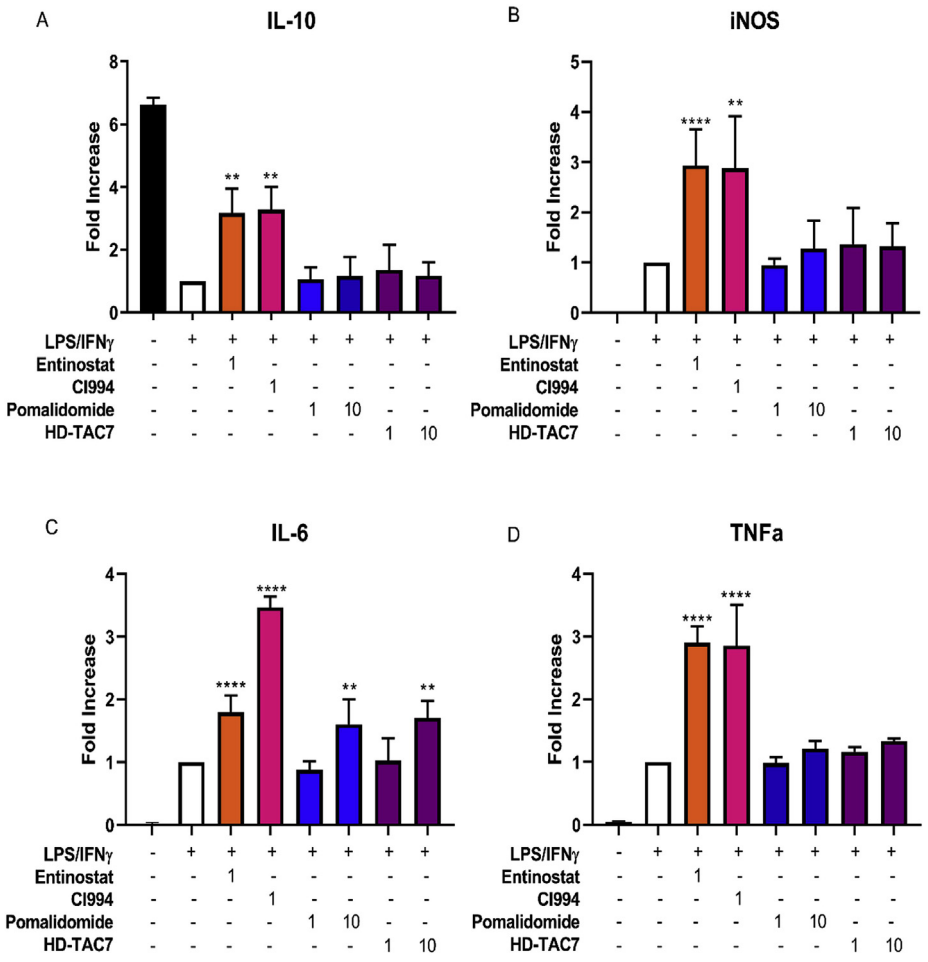

Fig. 5. Effects of Entinostat, CI994, pomalidomide and HD-TAC7 on pro- and anti-inflammatory gene expression of (A) IL-10, (B) iNOS, (C) IL-6 and (D) TNFα in RAW 264.7 macrophages. Cells were treated with the respective HDAC inhibitors at the indicated concentrations for 24h and stimulated with LPS/IFNγ for the last 4h of the experiments. Gene transcription was analyzed by RT-qPCR. For vehicle treatment, cells were pre-treated with a proportional dilution of the inhibitor solvent DMSO. Data shown is represented as mean values ± SD of 2−3 independent experiments. ****$p < 0.0001$ compared to vehicle treated-cells. **$p < 0.01$ compared to vehicle-treated cells.

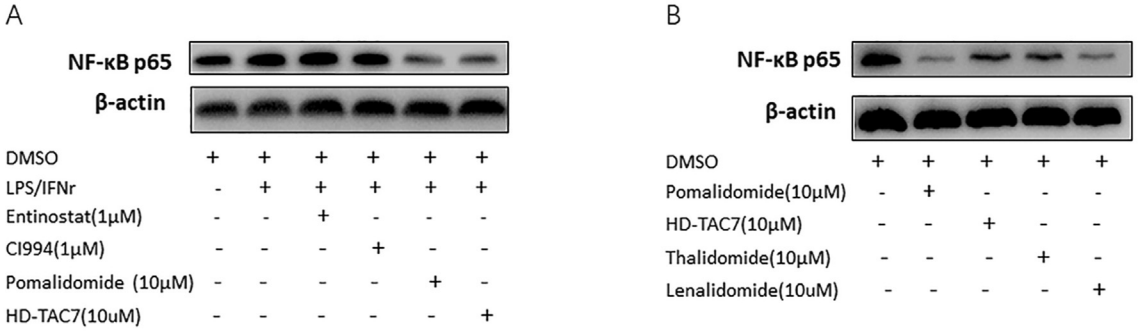

Fig. 6. (A) Western blot analysis of NF-κB p65 in RAW 264.7 macrophages. RAW 264.7 cells were incubated with Entinostat, CI994, pomalidomide or HD-TAC7 for 24h and stimulated with LPS and IFNα the last 4h of the experiment. (B) Analysis of NF-κB p65 protein level in RAW 264.7 macrophages using western blot. Cells were treated with pomalidomide, HD-TAC7, thalidomide or lenalidomide for 24h.

(q, $J = 8.0$ Hz, 2H).

4.1.10. tert-Butyl (2-(4-(5-(((benzyloxy)carbonyl)amino) pentanamido)benzamido)-5-fluorophenyl)carbamate(4d)

The product was obtained using synthetic procedure 1, starting from compound **3b**. White solid, yield 56%.^{1}H NMR (500 MHz, Chloroform-*d*) δ 8.95 (s, 1H), 8.21 (s, 1H), 7.88 (d, $J = 8.6$ Hz, 2H), 7.63 (d, $J = 8.4$ Hz, 2H), 7.48 (dd, $J = 8.7$, 5.8 Hz, 1H), 7.36−7.29 (m, 5H), 7.26−7.19 (m, 2H), 6.83 (td, $J = 8.8$, 2.8 Hz, 1H), 5.10 (s, 2H), 3.21 (p, $J = 6.2$ Hz, 2H), 2.37 (t, $J = 7.5$ Hz, 2H), 1.70 (dq, $J = 18.9$, 8.8, 8.0 Hz, 3H), 1.61−1.51 (m, 3H), 1.48 (s, 9H).

4.1.11. tert-Butyl (2-(4-(5-aminopentanamido)benzamido)phenyl) carbamate(5b)

The product was obtained using synthetic procedure 2, starting from compound **4b.** White oil, yield 95%.^{1}H NMR (500 MHz, Methanol-d_4) δ 7.94 (d, J = 8.7 Hz, 2H), 7.74 (d, J = 8.7 Hz, 2H), 7.60 (dd, J = 7.2, 1.8 Hz, 1H), 7.46–7.39 (m, 1H), 7.27–7.13 (m, 2H), 2.71 (t, J = 7.2 Hz, 2H), 2.44 (t, J = 7.4 Hz, 2H), 1.75 (p, J = 7.4 Hz, 2H), 1.62–1.55 (m, 2H), 1.50 (s, 9H).

4.1.12. tert-Butyl (2-(4-(6-aminohexanamido)benzamido)phenyl) carbamate(5c)

The product was obtained using synthetic procedure 2, starting from compound **4c.** White oil, yield 99%. ^{1}H NMR (500 MHz, Chloroform-d) δ 9.23 (s, 1H), 7.96 (s, 1H), 7.93–7.89 (m, 2H), 7.76 (dd, J = 7.9, 1.6 Hz, 1H), 7.64 (d, J = 8.4 Hz, 2H), 7.27 (d, J = 1.6 Hz, 1H), 7.18 (dtd, J = 25.1, 7.5, 1.7 Hz, 2H), 7.12 (s, 1H), 2.71 (t, J = 6.8 Hz, 2H), 2.35 (t, J = 7.4 Hz, 2H), 1.74–1.69 (m, 2H), 1.51 (s, 9H), 1.50–1.45 (m, 2H), 1.39 (qd, J = 7.6, 7.0, 4.3 Hz, 2H).

4.1.13. N-(2-aminophenyl)-4-(4-(2-((2-(2,6-dioxopiperidin-3-yl)-1,3-dioxoisoindolin-4-yl)amino)acetamido)butanamido) benzamide(7a)

The product was obtained using synthetic procedure 2 and 4, starting from compound **5a.** Yellow solid, yield 30%.^{1}H NMR (500 MHz, DMSO-d_6) δ 11.12 (s, 1H), 10.17 (s, 1H), 9.55 (s, 1H), 8.18 (t, J = 5.8 Hz, 1H), 7.94 (d, J = 8.5 Hz, 2H), 7.71 (d, J = 8.5 Hz, 2H), 7.64–7.56 (m, 1H), 7.16 (d, J = 7.8 Hz, 1H), 7.08 (d, J = 7.1 Hz, 1H), 7.00–6.94 (m, 2H), 6.88 (d, J = 8.6 Hz, 1H), 6.79 (d, J = 9.5 Hz, 1H), 6.60 (t, J = 8.1 Hz, 1H), 5.09 (dd, J = 12.8, 5.4 Hz, 1H), 4.88 (s, 2H), 3.95 (d, J = 5.6 Hz, 2H), 3.18 (dd, J = 5.9, 3.3 Hz, 3H), 2.95–2.84 (m, 1H), 2.66–2.52 (m, 2H), 2.38 (t, J = 7.5 Hz, 2H), 2.09–2.01 (m, 1H), 1.76 (p, J = 7.3 Hz, 2H). ^{13}C NMR (126 MHz, DMSO-d_6) δ 173.32, 171.75, 170.57, 169.18, 168.93, 167.80, 165.17, 146.28, 143.61, 142.53, 136.69, 132.52, 129.18, 129.13, 127.14, 126.84, 123.95, 118.55, 117.91, 116.74, 116.61, 111.43, 110.32, 55.39, 49.02, 45.63, 38.67, 34.28, 31.45, 25.48, 22.64. HRMS: $C_{32}H_{31}N_7O_7$, mass expected [M+H] $^+$ 626,23577, found 626,23578. HPLC: purity 99%, retention time 9.7 min.

4.1.14. N-(2-aminophenyl)-4-(5-(2-((2-(2,6-dioxopiperidin-3-yl)-1,3-dioxoisoindolin-4-yl)amino)acetamido)pentanamido) benzamide(7b)

The product was obtained using synthetic procedure 2 and 4, starting from compound **5b**. Yellow solid, yield 27%.^{1}H NMR (500 MHz, DMSO-d_6) δ 11.12 (s, 1H), 10.15 (s, 1H), 9.57 (s, 1H), 8.15 (t, J = 5.7 Hz, 1H), 7.94 (d, J = 8.6 Hz, 2H), 7.71 (d, J = 8.7 Hz, 2H), 7.62–7.56 (m, 1H), 7.16 (d, J = 7.9 Hz, 1H), 7.07 (d, J = 7.1 Hz, 1H), 7.00–6.93 (m, 2H), 6.87 (d, J = 8.6 Hz, 1H), 6.79 (dd, J = 7.9, 1.1 Hz, 1H), 6.64–6.55 (m, 1H), 5.08 (dd, J = 12.8, 5.4 Hz, 1H), 4.89 (s, 2H), 3.94 (d, J = 5.6 Hz, 2H), 3.16 (dq, J = 12.7, 6.6, 5.9 Hz, 2H), 2.96–2.82 (m, 1H), 2.68–2.52 (m, 2H), 2.36 (t, J = 7.3 Hz, 2H), 2.04 (dtd, J = 10.9, 5.9, 3.5 Hz, 1H), 1.61 (dt, J = 14.7, 7.2 Hz, 2H), 1.47 (dt, J = 13.9, 6.7 Hz, 2H). ^{13}C NMR (126 MHz, DMSO-d_6) δ 173.31, 172.01, 170.56, 169.17, 168.80, 167.80, 165.18, 146.30, 143.61, 142.56, 136.67, 132.52, 129.17, 127.13, 126.84, 123.95, 118.54, 117.92, 116.74, 116.60, 111.40, 110.31, 55.39, 49.02, 45.64, 38.81, 36.51, 31.45, 29.15, 22.87, 22.63. HRMS: $C_{33}H_{33}N_7O_7$, mass expected [M+H] $^+$ 640,25142, found 640,25156. HPLC: purity 99%, retention time 9.9 min.

4.1.15. N-(2-aminophenyl)-4-(6-(2-((2-(2,6-dioxopiperidin-3-yl)-1,3-dioxoisoindolin-4-yl)amino)acetamido)hexanamido) benzamide(7c)

The product was obtained using synthetic procedure 2 and 4, starting from compound **5c**. Yellow solid, yield 36%.^{1}H NMR (500 MHz, DMSO-d_6) δ 11.12 (s, 1H), 10.15 (s, 1H), 9.57 (s, 1H), 8.13 (t, J = 5.7 Hz, 1H), 7.94 (d, J = 8.3 Hz, 2H), 7.72 (d, J = 8.3 Hz, 2H), 7.60 (t, J = 7.8 Hz, 1H), 7.16 (d, J = 7.8 Hz, 1H), 7.07 (d, J = 7.0 Hz, 1H), 6.97 (q, J = 6.8, 5.6 Hz, 2H), 6.86 (d, J = 8.5 Hz, 1H), 6.79 (d, J = 7.9 Hz, 1H), 6.61 (t, J = 7.5 Hz, 1H), 5.09 (dd, J = 12.8, 5.4 Hz, 1H), 4.92 (s, 2H), 3.93 (d, J = 5.0 Hz, 2H), 3.12 (q, J = 6.5 Hz, 2H), 2.90 (td, J = 17.1, 15.2, 4.9 Hz, 1H), 2.66–2.53 (m, 2H), 2.35 (t, J = 7.5 Hz, 2H), 2.09–1.97 (m, 1H), 1.61 (p, J = 7.8 Hz, 2H), 1.46 (p, J = 7.1 Hz, 2H), 1.31 (p, J = 7.5, 6.6 Hz, 2H). ^{13}C NMR (126 MHz, DMSO-d_6) δ 173.31, 172.08, 170.56, 169.17, 168.71, 167.80, 165.17, 158.29,146.29, 143.48, 142.59, 132.52, 129.14, 127.13, 126.83, 124.01, 118.53, 117.90, 116.82, 116.66, 111.41, 110.30, 55.39, 49.01, 38.97, 36.84, 31.45, 29.36, 26.53, 25.14, 22.63. HRMS: $C_{34}H_{35}N_7O_7$, mass expected [M+H] $^+$ 654,26707, found 654,26697. HPLC: purity 99%, retention time 10.6 min.

4.1.16. N-(2-amino-4-fluorophenyl)-4-(5-(2-((2-(2,6-dioxopiperidin-3-yl)-1,3-dioxoisoindolin-4-yl)amino)acetamido) pentanamido)benzamide(7d)

The product was obtained using synthetic procedure 2 and 4, starting from compound **5b**. Yellow solid, yield 36%.^{1}H NMR (500 MHz, DMSO-d_6) δ 11.11 (s, 1H), 10.14 (s, 1H), 9.50 (s, 1H), 8.14 (t, J = 5.8 Hz, 1H), 7.93 (d, J = 8.5 Hz, 2H), 7.70 (d, J = 8.8 Hz, 2H), 7.61–7.54 (m, 1H), 7.10 (dd, J = 8.7, 6.3 Hz, 1H), 7.06 (d, J = 7.1 Hz, 1H), 6.95 (s, 1H), 6.86 (d, J = 8.6 Hz, 1H), 6.55 (dd, J = 11.2, 2.9 Hz, 1H), 6.37 (td, J = 8.5, 2.9 Hz, 1H), 5.07 (dd, J = 12.8, 5.4 Hz, 1H), 3.93 (s, 2H), 3.13 (q, J = 6.6 Hz, 2H), 2.97–2.82 (m, 1H), 2.63–2.52 (m, 2H), 2.35 (t, J = 7.3 Hz, 2H), 2.01 (dd, J = 15.9, 8.8 Hz, 1H), 1.59 (p, J = 7.4 Hz, 2H), 1.47 (q, J = 7.1 Hz, 2H). ^{13}C NMR (126 MHz, DMSO-d_6) δ 173.31, 172.01, 170.55, 169.16, 168.79, 167.79, 165.46, 162.35, 160.45, 155.99, 146.30,145.65, 142.58, 132.52, 129.04, 120.00, 118.43, 117.92, 114.33, 111.40, 110.31, 49.02, 45.63, 38.80, 36.49, 31.45, 28.68, 22.57. HRMS: $C_{33}H_{32}FN_7O_7$, mass expected [M+H] $^+$ 658,242, found 658,24164. HPLC: purity 98%, retention time 10.3 min.

4.1.17. N-(2-aminophenyl)-4-(4-((2-(2,6-dioxopiperidin-3-yl)-1,3-dioxoisoindolin-4-yl)amino)butanamido)benzamide(9a)

The product was obtained using synthetic procedure 3 and 4, starting from compound **5a**. Yellow solid, yield 17%.^{1}H NMR (500 MHz, DMSO-d_6) δ 11.09 (s, 1H), 10.29 (s, 1H), 9.60 (s, 1H), 7.93 (d, J = 8.7 Hz, 2H), 7.70 (d, J = 8.7 Hz, 2H), 7.59 (dd, J = 8.4, 7.2 Hz, 1H), 7.18–7.13 (m, 2H), 7.03 (d, J = 7.0 Hz, 1H), 6.99–6.93 (m, 1H), 6.77 (dd, J = 8.0, 1.2 Hz, 1H), 6.69 (t, J = 5.9 Hz, 1H), 6.63–6.56 (m, 1H), 5.04 (dd, J = 12.8, 5.4 Hz, 1H), 4.88 (s, 2H), 3.45–3.39 (m, 2H), 2.88 (tdd, J = 14.4, 13.9, 5.7, 4.2 Hz, 1H), 2.64–2.52 (m, 2H), 2.47 (t, J = 7.2 Hz, 2H), 2.05–1.97 (m, 1H), 1.91 (p, J = 7.1 Hz, 2H). HRMS: $C_{30}H_{28}N_6O_6$, mass expected [M+H] $^+$ 569,21431, found 569,21423. HPLC: purity 91%, retention time 10.6 min.

4.1.18. N-(2-aminophenyl)-4-(5-((2-(2,6-dioxopiperidin-3-yl)-1,3-dioxoisoindolin-4-yl)amino)pentanamido)benzamide(9b)

The product was obtained using synthetic procedure 3 and 4, starting from compound **5b**. Yellow solid, yield 38%.^{1}H NMR (500 MHz, DMSO-d_6) δ 11.11 (s, 1H), 10.18 (s, 1H), 9.56 (s, 1H), 7.94 (d, J = 8.6 Hz, 2H), 7.71 (d, J = 8.7 Hz, 2H), 7.60–7.55 (m, 1H), 7.14 (dd, J = 15.1, 8.0 Hz, 2H), 7.03 (d, J = 7.0 Hz, 1H), 6.97 (d, J = 16.7 Hz, 1H), 6.78 (d, J = 8.0 Hz, 1H), 6.65–6.56 (m, 2H), 5.06 (dd, J = 12.8, 5.5 Hz, 1H), 4.89 (s, 2H), 3.42–3.36 (m, 2H), 2.95–2.82 (m, 1H), 2.67–2.53 (m, 2H), 2.42 (t, J = 7.1 Hz, 2H), 2.10–1.97 (m, 1H), 1.67 (dq, J = 26.5, 8.1, 7.6 Hz, 4H). ^{13}C NMR (126 MHz, DMSO-d_6) δ 173.31, 171.98, 170.60, 169.38, 167.78, 165.87, 165.15, 156.02, 146.84, 143.60, 142.52, 136.72, 132.71, 129.21, 129.13, 127.12, 126.84, 123.95, 118.56, 117.66, 116.73, 116.58, 115.60, 114.34, 110.86, 109.52, 49.00, 42.01, 36.56, 31.44, 28.77, 22.65. HRMS: $C_{31}H_{30}N_6O_6$, mass expected [M+H] $^+$ 583,22996, found 583,22986. HPLC: purity 96%, retention time 11.1 min.

4.1.19. N-(2-aminophenyl)-4-(6-((2-(2,6-dioxopiperidin-3-yl)-1,3-dioxoisoindolin-4-yl)amino)hexanamido)benzamide(9c)

The product was obtained using synthetic procedure 3 and 4, starting from compound **5c**. Yellow solid, yield 31%.^{1}H NMR (500 MHz, DMSO-d_6) δ 11.10 (s, 1H), 10.13 (s, 1H), 9.55 (s, 1H), 7.93 (d, J = 8.4 Hz, 2H), 7.70 (d, J = 8.5 Hz, 2H), 7.61–7.54 (m, 1H), 7.13 (dd, J = 21.9, 8.8 Hz, 2H), 7.02 (d, J = 6.6 Hz, 1H), 6.96 (t, J = 7.6 Hz, 1H), 6.78 (d, J = 8.8 Hz, 1H), 6.65–6.51 (m, 2H), 5.05 (dd, J = 12.7, 4.8 Hz, 1H), 4.87 (s, 2H), 3.21–3.11 (m, 2H), 2.94–2.82 (m, 1H), 2.58 (dd, J = 17.4, 3.2 Hz, 2H), 2.36 (t, J = 7.1 Hz, 2H), 2.08–1.98 (m, 1H), 1.69–1.58 (m, 4H), 1.46–1.35 (m, 2H). ^{13}C NMR (126 MHz, DMSO-d_6) δ 173.32, 172.08, 170.61, 169.41, 167.78, 165.17, 146.88, 143.61, 142.58, 136.77, 132.67, 129.15, 129.12, 127.13, 123.96, 118.54, 117.69, 116.73, 116.60, 110.86, 109.46, 48.99, 42.18, 36.87, 31.45, 29.00, 26.47, 25.23, 22.62. HRMS: $C_{32}H_{32}N_6O_6$, mass expected $[M+H]^+$ 597,24561, found 597,24564. HPLC: purity 98%, retention time 11.5 min.

4.2. HDAC inhibition study

Black 96-well flat-bottom microplates (Corning® Costar®, Corning Incorporated, NY) were used. Human recombinant C-terminal FLAG-tag, C-terminal His-tag HDAC1 (BPS Bioscience, Catalog #: 50051), Human recombinant C-terminal FLAG-tag HDAC2 (BPS Bioscience, Catalog #: 50052) or human recombinant C-terminal His-tag HDAC3/NcoR2 (BPS Bioscience, Catalog #: 50003) were diluted in incubation buffer (25 mM Tris-HCl, pH 8.0, 137 mM NaCl, 2.7 mM KCl, 1 mM MgCl, 0.01% Triton-X and 1 mg/mL BSA). 40 μL of this dilution was incubated with 10 μL of different concentrations of inhibitors in 10% DMSO/incubation buffer and 50 μL of the fluorogenic Boc-Lys(ε-Ac)-AMC (20 mM, Bachem, Germany) at 37 °C. After 90 min incubation time 50 μL of the stop solution (25 mM Tris-HCl (pH 8), 137 mM NaCl, 2.7 mM KCl, 1 mM $MgCl_2$, 0.01% Triton-X, 6.0 mg/mL trypsin (porcine pancreas Type IX-S, lyophilized powder, 13,000–20,000 BAEE units/mg protein, Sigma Aldrich) and 200 μM vorinostat) was added. After a following incubation at 37 °C for 30 min, the fluorescence was measured on a Synergy H1 Platereader (BioTek, USA) with a gain of 70, an excitation wavelength of 370 nm and an emission wavelength of 460 nm. GraphPad Prism 5.0 (GraphPad Software, Inc.) was used for the determination of the DC_{50} of each inhibitor. Nonlinear regression was used for data fitting.

4.3. Cell viability

4.3.1. Cell culture

RAW 264.7 macrophages were obtained from the American Type Culture Collection (ATCC; Wesel, Germany) and cultured in 96-well plate or flasks (Costar Europe, Badhoevedrop, The Netherlands) at 37 °C under 5% CO_2/95% air in Dulbecco's Modification of Eagle's Medium (DMEM) containing GlutaMAX™ (Gibco® by life Technologies, Bleiswijk, The Netherlands) supplemented with 10% (v/v) heated fetal bovine serum (FBS; Invitrogen, Breda, The Netherlands), 2 mM additional GlutaMAX™ (Gibco® by life Technology, Bleiswijk, The Netherlands), 100U/ml penicillin (Gibco® by life Technologies, Bleiswijk, The Netherlands) and 100 μg/ml streptomycin (Gibco® by life Technologies, Bleiswijk, The Netherlands). RAW 264.7 cells were used between passage 5 and 16.

4.3.2. MTS assay

RAW264.7 cells were seeded in 96-well plate at the concentration of 25,000 cells/cm^2. The next day, medium was replaced with fresh medium containing HDAC inhibitors at the indicated concentrations. After 24h incubation at 37 °C, 20 μl CellTiter 96 AQ_{ueous} One Solution reagent (Promega) was added to each well. The cells were incubated at 37 °C for 2h in the dark. The absorbance at 490 nM was measured using a Synergy H1 plate reader. The results were plotted as % of control.

4.3.3. Western blotting

RAW264.7 cells were washed twice with ice-cold DPBS and subsequently lysed in ice-cold lysis buffer (25 mM Hepes, 5 mM $MgCl_2$, 5 mM EDTA, 0.5% Triton X-100 and protease inhibitors (#88266; Thermo Scientific, Rockford, IL, USA)). Protein concentrations were determined by a Pierce BCA Protein Assay Kit (Thermo Fisher Scientific, USA) according to the manufacturer's protocol. Samples were separated by NuPAGE™ 4–12% Bis-Tris gel (Invitrogen, Carlsbad, Canada), and transferred with a Trans-Blot Electrophoretic Transfer system (Bio-Rad Laboratories) onto a polyvinylidene difluoride membrane (PVDF; Bio-Rad Laboratories). The membrane was blocked at room temperature for 1h in PBS/0.1% Tween 20 (Sigma-Aldrich; solution referred to as PBST) containing 5% skimmed milk (Campina, Friesland, The Netherlands) and subsequently incubated overnight at 4 °C with the appropriate primary antibody in 5% BSA (Sigma-Aldrich) or 5% skimmed milk in PBST. The following primary antibodies and dilutions were used: HDAC1 (1:2000), HDAC2 (1:2000), HDAC3 (1:2000), NF-κB p65 (1:2500), acH3K27(1:1000) and β-actin (1:10000); all from CellSignaling, Leiden, The Netherlands. Membranes were washed in PBST and incubated at room temperature for 1h with peroxidase-conjugated secondary antibodies. The following secondary antibodies were used: goat anti-rabbit IgG/HRP, and rabbit anti-mouse IgG/HRP (all 1:2000; DakoCytomation, Glostrup, Denmark). The bands were visualized using the VisiGlo™ Prime HRP Chemiluminescenct Substrate Kit (AMRESCO, Solon, OH, USA). For the western blot of 0.001μM–30μM HD-TAC7-treated RAW264.7 cells were worked up according to the protocol above until blocking the membrane. The membrane was blocked at room temperature for 1h in Odyssey blocking buffer. The primary antibodies and dilutions were used above, while the fluorescent secondary antibodies were used as following: IRDye 680RD Goat anti-Mouse IgG (H + L) (1:10000, Fisher Scientific) and IRDye® 800CW Goat anti-Rabbit IgG (1:10000, LI-COR Biosciences, UK). The bands were visualized using Odyssey® CLx Blot Scanner (LI-COR Biosciences, UK).

4.3.4. RT-qPCR

RAW264.7 cells were washed twice with Dulbecco's Phosphate-buffered Saline (DPBS, Gibco® by life Technologies, Bleiswijk, The Netherlands) and total RNA was isolated by Maxwell® 16 LEV simplyRNA Tissue Kit (Promega) according to the manufacturer's protocol. RNA concentration (OD_{260}) and purity (OD_{260}/OD_{280}) were measured by NanoDrop ND-1000 UV–Vis spectrophotometer (NanoDrop Technologies, Wilmington, DE, USA). Then, RNA was reverse transcribed to cDNA using the Reverse Transcription Kit (#A3500, Promega). 10 ng of cDNA, 5uL 2x SensiMix SYBR Lo-ROX and 0.4 μL primers were applied for each RT-qPCR, which was performed on a QuantStudio™ 7 Flex System. For each sample, the real-time PCR was performed in duplicate. Data analysis was performed with QuantStudio™ Real-Time PCR Software. Gene expression levels were normalized to the expression of the reference gene glyceralde-3-phosphate dehydrogenase (GAPDH), which was not influenced by the experimental conditions resulting in the ΔC_t value. Gene expression levels were calculated by the comparative C_t method ($2^{-\Delta\Delta Ct}$) [38].

Primers for qRT-PCR were as follows:

GAPDH forward, 5′- ACAGTCCATGCCATCACTGC-3';
GAPDH reverse, 5′- GATCCACGACGGACACATTG-3';
IL-10 forward, 5′- ATAACTGCACCCACTTCCCAGTC-3';
IL-10 reverse, 5′- CCCAAGTAACCCTTAAAGTCCTGC-3';
IL-6 forward, 5′- TGATGCTGGTGACAACCACGGC-3';

IL-6 reverse, 5′- TAAGCCTCCGACTTGTGAAGTGGTA-3';
TNFα forward, 5′- CATCTTCTCAAAATTCGAGTGACAA-3';
TNFα reverse, 5′- GAGTAGACAAGGTACAACCC-3';
miNOS forward, 5′- CTATCAGGAAGAAATGCAGGAGAT-3';
miNOS reverse, 5′- GAGCACGCTGAGTACCTCATT-3';

Declaration of competing interest

The authors declare that they have no known competing financial interests or personal relationships that could have appeared to influence the work reported in this paper.

Acknowledgement

We acknowledge the Chinese Scholarship Council (CSC) for providing a scholarship to Fangyuan Cao (grant ID: 201606170109) and to Deng Chen (grant ID: 201907720019).

Appendix. Supplementary data

Supplementary data associated with this article can be found in the online version, at https://doi.org/10.1016/j.ejmech.2020.112800. These data include MOL files and InChiKeys of the most important compounds described in this article.

References

[1] E. Seto, M. Yoshida, Erasers of histone acetylation: the histone deacetylase enzymes, Cold Spring Harb. Perspect. Biol. 6 (2014), https://doi.org/10.1101/cshperspect.a018713.
[2] H.-T. Qin, H.-Q. Li, F. Liu, Selective histone deacetylase small molecule inhibitors: recent progress and perspectives, Expert Opin. Ther. Pat. 27 (2016) 1–15, https://doi.org/10.1080/13543776.2017.1276565.
[3] M. Dokmanovic, C. Clarke, P.A. Marks, Histone deacetylase inhibitors: overview and perspectives, Mol. Canc. Res. 5 (2007) 981–989, https://doi.org/10.1158/1541-7786.MCR-07-0324.
[4] G.P. Delcuve, D.H. Khan, J.R. Davie, Roles of histone deacetylases in epigenetic regulation: emerging paradigms from studies with inhibitors, Clin. Epigenet. 4 (2012) 5, https://doi.org/10.1186/1868-7083-4-5.
[5] A. Villagra, E.M. Sotomayor, E. Seto, Histone deacetylases and the immunological network: implications in cancer and inflammation, Oncogene 29 (2010) 157–173, https://doi.org/10.1038/onc.2009.334.
[6] F.J.D. Martijn, R.H. Zwinderman, Fangyuan Cao, Acetylation and methylation in asthma, COPD, and lung cancer martijn, in: Top Med Chem, Springer Nature, Switzerland AG, 2019, https://doi.org/10.1007/7355.
[7] T. Van Den Bosch, Targeting transcription factor lysine acetylation in inflammatory airway diseases 9 (2017) 1013–1028, https://doi.org/10.2217/epi-2017-0027.
[8] N.G.J. Leus, M.R.H. Zwinderman, F.J. Dekker, Histone deacetylase 3 (HDAC 3) as emerging drug target in NF-κB-mediated inflammation, Curr. Opin. Chem. Biol. 33 (2016) 160–168, https://doi.org/10.1016/j.cbpa.2016.06.019.
[9] M.R.H. Zwinderman, S. de Weerd, F.J. Dekker, Targeting HDAC complexes in asthma and COPD, Epigenomes 3 (2019) 19, https://doi.org/10.3390/epigenomes3030019.
[10] N.G.J. Leus, T. van den Bosch, P.E. van der Wouden, K. Krist, M.E. Ourailidou, N. Eleftheriadis, L.E.M. Kistemaker, S. Bos, R.A.F. Gjaltema, S.A. Mekonnen, R. Bischoff, R. Gosens, H.J. Haisma, F.J. Dekker, HDAC1-3 inhibitor MS-275 enhances IL10 expression in RAW264.7 macrophages and reduces cigarette smoke-induced airway inflammation in mice, Sci. Rep. 7 (2017) 45047, https://doi.org/10.1038/srep45047.
[11] N.G.J. Leus, P.E. Van Der Wouden, T. Van Den Bosch, W.T.R. Hooghiemstra, M.E. Ourailidou, L.E.M. Kistemaker, R. Bischoff, R. Gosens, H.J. Haisma, F.J. Dekker, HDAC 3-selective inhibitor RGFP966 demonstrates anti-inflammatory properties in RAW 264.7 macrophages and mouse precision-cut lung slices by attenuating NF-κB p65 transcriptional activity, Biochem. Pharmacol. 108 (2016) 58–74, https://doi.org/10.1016/j.bcp.2016.03.010.
[12] F. Cao, M. Zwinderman, R. van Merkerk, P. Ettema, W. Quax, F.J. Dekker, Inhibitory selectivity among class I HDACs has a major impact on inflammatory gene expression in macrophages, Eur. J. Med. Chem. 177 (2019) 457–466, https://doi.org/10.1016/j.ejmech.2019.05.038.
[13] A.C. Lai, C.M. Crews, Induced protein degradation: an emerging drug discovery paradigm, Nat. Rev. Drug Discov. 16 (2017) 101–114, https://doi.org/10.1038/nrd.2016.211.
[14] S.-L. Paiva, C.M. Crews, Targeted protein degradation: elements of PROTAC design, Curr. Opin. Chem. Biol. 50 (2019) 111–119, https://doi.org/10.1016/j.cbpa.2019.02.022.
[15] I. Churcher, Protac-induced protein degradation in drug discovery: breaking the rules or just making new ones? J. Med. Chem. (2018) https://doi.org/10.1021/acs.jmedchem.7b01272.
[16] A.N. B, C.M. C, Matthieu Schapira, Matthew F. Calabrese, Targeted protein degradation: expanding the toolbox, Nat. Rev. Drug Discov. (2019), https://doi.org/10.1038/s41573-019-0047-y.
[17] D.P. Bondeson, B.E. Smith, G.M. Burslem, A.D. Buhimschi, J. Hines, S. Jaime-Figueroa, J. Wang, B.D. Hamman, A. Ishchenko, C.M. Crews, Lessons in PROTAC design from selective degradation with a promiscuous warhead, Cell Chem. Biol. 25 (2018) 78–87, https://doi.org/10.1016/j.chembiol.2017.09.010, e5.
[18] Z.I. Bassi, M.C. Fillmore, A.H. Miah, T.D. Chapman, C. Maller, E.J. Roberts, L.C. Davis, D.E. Lewis, N.W. Galwey, K.E. Waddington, V. Parravicini, A.L. Macmillan-Jones, C. Gongora, P.G. Humphreys, I. Churcher, R.K. Prinjha, D.F. Tough, Modulating PCAF/GCN5 immune cell function through a PROTAC approach, ACS Chem. Biol. 13 (2018) 2862–2867, https://doi.org/10.1021/acschembio.8b00705.
[19] M. Konstantinidou, J. Li, B. Zhang, Z. Wang, S. Shaabani, F. Ter Brake, K. Essa, A. Dömling, PROTACs– a game-changing technology, Expet Opin. Drug Discov. (2019) 1–14, https://doi.org/10.1080/17460441.2019.1659242, 00.
[20] K. Yang, Y. Song, H. Xie, H. Wu, Y.T. Wu, E.D. Leisten, W. Tang, Development of the first small molecule histone deacetylase 6 (HDAC6) degraders, Bioorg. Med. Chem. Lett 28 (2018) 2493–2497, https://doi.org/10.1016/j.bmcl.2018.05.057.
[21] Y. R, Zixuan An, Wenxing Lv, Shang Su, Wei Wu, Developing potent PROTACs tools for selective degradation of HDAC6 protein, Protein Cell (2019) 8–11, https://doi.org/10.1007/s13238-018-0602-z.
[22] H. Wu, K. Yang, Z. Zhang, E.D. Leisten, Z. Li, H. Xie, J. Liu, K.A. Smith, Z. Novakova, C. Barinka, W. Tang, Development of multifunctional histone deacetylase 6 degraders with potent antimyeloma activity, J. Med. Chem. (2019), https://doi.org/10.1021/acs.jmedchem.9b00516 acs.jmedchem.9b00516.
[23] M. Schiedel, D. Herp, S. Hammelmann, S. Swyter, A. Lehotzky, D. Robaa, J. Oláh, J. Ovádi, W. Sippl, M. Jung, Chemically induced degradation of sirtuin 2 (Sirt2) by a proteolysis targeting chimera (PROTAC) based on sirtuin rearranging ligands (SirReals), J. Med. Chem. 61 (2018) 482–491, https://doi.org/10.1021/acs.jmedchem.6b01872.
[24] F.F. Wagner, M. Lundh, T. Kaya, P. McCarren, Y.L. Zhang, S. Chattopadhyay, J.P. Gale, T. Galbo, S.L. Fisher, B.C. Meier, A. Vetere, S. Richardson, N.G. Morgan, D.P. Christensen, T.J. Gilbert, J.M. Hooker, M. Leroy, D. Walpita, T. Mandrup-Poulsen, B.K. Wagner, E.B. Holson, An isochemogenic set of inhibitors to define the therapeutic potential of histone deacetylases in β-cell protection, ACS Chem. Biol. 11 (2016) 363–374, https://doi.org/10.1021/acschembio.5b00640.
[25] J. Roche, P. Bertrand, Inside HDACs with more selective HDAC inhibitors, Eur. J. Med. Chem. 121 (2016) 451–483, https://doi.org/10.1021/jm400179b.
[26] A. Suraweera, K.J. O'Byrne, D.J. Richard, Combination therapy with histone deacetylase inhibitors (HDACi) for the treatment of cancer: achieving the full therapeutic potential of HDACi, Front. Oncol. 8 (2018) 1–15, https://doi.org/10.3389/fonc.2018.00092.
[27] B.E.L. Lauffer, R. Mintzer, R. Fong, S. Mukund, C. Tam, I. Zilberleyb, B. Flicke, A. Ritscher, G. Fedorowicz, R. Vallero, D.F. Ortwine, J. Gunzner, Z. Modrusan, L. Neumann, C.M. Koth, J.S. Kaminker, C.E. Heise, P. Steiner, Histone deacetylase (HDAC) inhibitor kinetic rate constants correlate with cellular histone acetylation but not transcription and cell viability, J. Biol. Chem. 288 (2013) 26926–26943, https://doi.org/10.1074/jbc.M113.490706.
[28] C.J. Chou, D. Herman, J.M. Gottesfeld, Pimelic diphenylamide 106 is a slow, tight-binding inhibitor of class I histone deacetylases, J. Biol. Chem. 283 (2008) 35402–35409, https://doi.org/10.1074/jbc.M807045200.
[29] H.-Y. Hsieh, H.-C. Chuang, F.-H. Shen, K. Detroja, L.-W. Hsin, C.-S. Chen, Targeting breast cancer stem cells by novel HDAC3-selective inhibitors, Eur. J. Med. Chem. 140 (2017) 42–51, https://doi.org/10.1016/j.ejmech.2017.08.069.
[30] Detlef Schuppan, Christoph Herold, Marion Gansmayer, Matthias Ocker, K.-H. Thierauch, Preparation of N-Aryl Benzamides as Histone Deacetylase Inhibitors, 2014. WO 2004/058234.
[31] C.E. Powell, Y. Gao, L. Tan, K.A. Donovan, R.P. Nowak, A. Loehr, M. Bahcall, E.S. Fischer, P.A. Jänne, R.E. George, N.S. Gray, Chemically induced degradation of anaplastic lymphoma kinase (ALK), J. Med. Chem. 61 (2018) 4249–4255, https://doi.org/10.1021/acs.jmedchem.7b01655.
[32] B. Zhou, J. Hu, F. Xu, Z. Chen, L. Bai, E. Fernandez-Salas, M. Lin, L. Liu, C.Y. Yang, Y. Zhao, D. McEachern, S. Przybranowski, B. Wen, D. Sun, S. Wang, Discovery of a small-molecule degrader of bromodomain and extra-terminal (BET) proteins with picomolar cellular potencies and capable of achieving tumor regression, J. Med. Chem. 61 (2018) 462–481, https://doi.org/10.1021/acs.jmedchem.6b01816.
[33] B. Wang, S. Wu, J. Liu, K. Yang, H. Xie, W. Tang, Development of selective small molecule MDM2 degraders based on nutlin, Eur. J. Med. Chem. 176 (2019) 476–491, https://doi.org/10.1016/j.ejmech.2019.05.046.
[34] S.-L. Paiva, C.M. Crews, Targeted protein degradation: elements of PROTAC design, Curr. Opin. Chem. Biol. 50 (2019) 111–119, https://doi.org/10.1016/j.cbpa.2019.02.022.
[35] J. Mohseni, Z.A.M.H. Zabidi-Hussin, T.H. Sasongko, Histone deacetylase inhibitors as potential treatment for spinal muscular atrophy, Genet. Mol. Biol. 36 (2013) 299–307, https://doi.org/10.1590/S1415-47572013000300001.
[36] A. Yuliana, H.F. Jheng, S. Kawarasaki, W. Nomura, H. Takahashi, T. Ara, T. Kawada, T. Goto, Β-adrenergic receptor stimulation revealed a novel

regulatory pathway via suppressing histone deacetylase 3 to induce uncoupling protein 1 expression in mice beige adipocyte, Int. J. Mol. Sci. 19 (2018) 1–15, https://doi.org/10.3390/ijms19082436.
[37] Y. Shirai, N. Saito, T. Uwagawa, H. Shiba, T. Horiuchi, R. Iwase, K. Haruki, T. Ohashi, K. Yanaga, Pomalidomide promotes chemosensitization of pancreatic cancer by inhibition of NF-κB, Oncotarget 9 (2018) 15292–15301, https://doi.org/10.18632/oncotarget.24577.
[38] K.J. Livak, T.D. Schmittgen, Analysis of relative gene expression data using real-time quantitative PCR and the 2-ΔΔCT method, Methods 25 (2001) 402–408, https://doi.org/10.1006/meth.2001.1262.